

# Numerical Study on Turbine Wakes in Wind Farms

Mahmoud F. Nofal<sup>1</sup>, Ali M. AbdelSalam<sup>2</sup>, W.A. El-Askary<sup>3</sup>, Osama E. Abdellatif<sup>4</sup> and Samir S. Ayad<sup>4</sup>  
Mechanical Engineering Department, Shoubra Faculty of Engineering, Benha University, Egypt

This paper presents a study of the wake behavior behind horizontal axis wind turbines (WTs) using CFD. Simulations are carried out, to identify the most effective WT's distribution that improves the performance of the wind farm as a whole. The rotors are modeled by using the actuator disk theory and the simulations are performed using ANSYS FLUENT. An assumed land space of 13D width and 20D length is considered for the WT's arrangement, where D is the rotor diameter. Simulations are performed for various configurations with different distances between WT's (6D, 8D and 10D) and three prevailing wind directions. Results show that the changes in WT's distribution significantly affect the wind power available in the wind farm. Staggered configuration of 6D separation distance is found to have the best power output, even with less number of WT's. It is also observed that the change in the wind direction blowing to the wind farm can lead to more than 100% change in the power output especially for non-staggered configurations.

## I. Nomenclature

D	Diameter of the rotor	m
u	Wind speed	m/s
$U_0$	Ambient wind velocity	m/s
$C_L$	Lift coefficient	
$C_P$	Power coefficient	
$C_T$	Thrust coefficient	
P	Power	kW
$\rho$	Air density	kg/m <sup>3</sup>
T	Thrust	N
x,y,z	Cartesian coordinates	m
$\Delta p$	Pressure drop across the turbine disc	N/m <sup>2</sup>
k	Kinetic energy of turbulence	m <sup>2</sup> /s <sup>2</sup>
$\epsilon$	Rate of dissipation of turbulence energy	m <sup>2</sup> /s <sup>3</sup>

---

<sup>1</sup> Graduated student, Mechanical Engineering Department, Shoubra Faculty of Engineering, Benha University, Egypt

<sup>2</sup> Assistant Professor, Mechanical Power Engineering Department, Faculty of Engineering, Shebin El-Kom, Menoufia University, Egypt

<sup>3</sup> Professor, Mechanical Power Engineering Department, Faculty of Engineering, Shebin El-Kom, Menoufia University, Egypt

<sup>4</sup> Professor, Mechanical Engineering Department, Shoubra Faculty of Engineering, Benha University, Egypt

## II. Introduction

Wind energy has become a very important branch of renewable energy for electricity production. Wind farms are necessary for large wind power plants. To make wind power economically feasible, it is important to maximize the efficiency of converting wind energy into mechanical energy for turbines located downstream of each other's. Subsequently, the wind turbines distribution in a wind farm is a very important parameter in wind energy projects [1].

The wakes behind wind turbines have significant effects on the downstream flow, which is characterized by low wind speed and more intensive turbulence than that of the free stream flow [2]. To improve the performance of the wind farm, it is necessary to adjust the most effective separation distance between turbines. However, the experimental work on such a problem is very expensive and highly complex. Alternatively, the Computational Fluid Dynamics (CFD) offers a lower cost and shorter time method compared to experimental investigations. CFD, which uses Reynolds Averaged Navier Stokes (RANS) equations, is regarded as a powerful tool for understanding interactions between wind turbines. Choi et al [3] and Jourieh et al [4] have performed analyses of multiple wakes using two or more wind turbines. They demonstrated that the separation distance is a very important factor in designing wind farms, and that lower upstream wind speed leads to higher percent of power loss. El Askary et al [5] studied the interaction between wind turbines working in thermally stratified Atmospheric Boundary Layer ABL; where the unstable ABL gave smaller wake region as compared to stable ABL conditions. Furthermore, experimental measurements and numerical techniques using a modified k-ε model were performed on the wake behavior by Abdelsalam et al [6-7]. Results showed a good agreement between the proposed CFD method and the experimental data. It is worth mentioning that, detached eddy simulation and large eddy simulation approaches are also performed for wind turbine wake studies [8-9]. However, both techniques require more time and more computational efforts.

In the present paper simulations using a modified k-ε model for the turbulent flow around the WTs, first suggested by El Kasmi and Masson [10] have been performed. Several configurations of the WTs with different separation distances between the turbines (6D, 8D and 10D) and different wind directions have been predicted, to optimize the layout of the wind farm.

## III. Mathematical model

The proposed work is devoted to study the interaction between wind turbines in wind farm. The numerical simulation is implemented using the 2-D steady Reynolds Averaged Navier Stokes equations. The turbine rotor is modeled by using the actuator disk theory. The effect of the rotor is represented by momentum source as a pressure drop caused by the rotor, which is given by:

$$\Delta p = 0.5 \rho C_T U_0^2 \quad (1)$$

where,  $\rho$  is the air density,  $C_T$  is the thrust coefficient which is assumed constant across the actuator disk, and  $U_0$  is the undisturbed wind velocity at hub height.

The EL Kasmi turbulence model has proven a significant improvement in the wind turbine wake predictions [10]. Hence, it is used in the present work to treat the turbulence and close the solution of equations. The transport equation for the turbulence kinetic energy is given by:

$$\frac{\partial \rho k u_j}{\partial x_j} = \frac{\partial}{\partial x_j} \left[ \left( \mu + \frac{\mu_t}{\sigma_k} \right) \frac{\partial k}{\partial x_j} \right] + P_t - \rho \varepsilon \quad (2)$$

where,  $k$  is turbulence kinetic energy,  $\sigma_k$  is the Prandtl number for turbulence kinetic energy and  $P_t$  and  $\varepsilon$  are the production and the dissipation rates of the turbulence kinetic energy, respectively. The production rate  $P_t$  is calculated by:

$$P_t = \mu_t \left( \frac{\partial u_i}{\partial x_j} + \frac{\partial u_j}{\partial x_i} \right) \frac{\partial u_i}{\partial x_j}, \quad (3)$$

The turbulent viscosity  $\mu_t$  is calculated by:

$$\mu_t = \rho C_\mu \frac{k^2}{\varepsilon} \left( \frac{\pi}{2} - \theta \right) \quad (4)$$

The transport equation of turbulence dissipation rate  $\varepsilon$  can be written as

$$\frac{\partial \rho \varepsilon u_j}{\partial x_j} = \frac{\partial}{\partial x_j} \left[ \left( \mu + \frac{\mu_t}{\sigma_\varepsilon} \right) \frac{\partial \varepsilon}{\partial x_j} \right] + C_{1\varepsilon} \frac{\varepsilon}{k} P_t - \rho C_{2\varepsilon} \frac{\varepsilon^2}{k} + P_\varepsilon \quad (5)$$

where,  $P_\varepsilon$  is additional source term given by

$$P_\varepsilon = C_{4\varepsilon} \frac{P_t^2}{\rho k} \quad (6)$$

This source term describes the energy transfer rate from large scale turbulence rate to small scale turbulence rate in the near wake of the wind turbine. It is expressed by 0.25 D volume upstream and downstream of the turbine as proposed in [10]. In order to control the development of the turbulence kinetic energy for neutral atmospheric flow more effective values of the model constants are taken according to Crespo et al; [11], as follows

$$\sigma_k = 1; \quad \sigma_\varepsilon = 1.3; \quad C_{1\varepsilon} = 1.176; \quad C_{2\varepsilon} = 1.92; \quad C_\mu = 0.033; \quad C_{4\varepsilon} = 0.37$$

#### IV. Numerical method

The governing equations are solved numerically by employing **ANSYS FLUENT 16** in steady two-dimensional planar mode, while the discretization process is performed using the control-volume-based technique. Moreover, the **SIMPLE** algorithm is used. Besides, second-order upwind scheme is used for all dependent variables. The source terms are programmed in C language, and have been implemented to the governing equations through user defined function UDF, when required. In the present work, the two-dimensional domain presented in Fig. 1 is used in case of single wake, for turbulence model validation. However, for multiple wakes produced by a wind farm, the computational domain presented in Fig. 2 is used. A structured surface mesh of the computational domain is created using ANSYS ICEM program. The velocity inlet boundary condition is implemented at the domain inlet which is positioned 5D upstream of the turbine rotor for all cases. The axial velocity component, turbulence kinetic energy  $k$  and dissipation rate  $\varepsilon$  are fed with uniform values equivalent to that prevailing at hub height. The distance downstream the last wind turbine rotor is large enough not less than 15D for all cases, so that the atmospheric pressure is assumed to attain its value at that distance. Hence, the pressure outlet boundary condition is applied at the outlet domain, with zero gauge pressure. The lateral sides are located far away from the turbine rotor, so that, symmetry boundary condition is suitable assumption for the lateral sides.

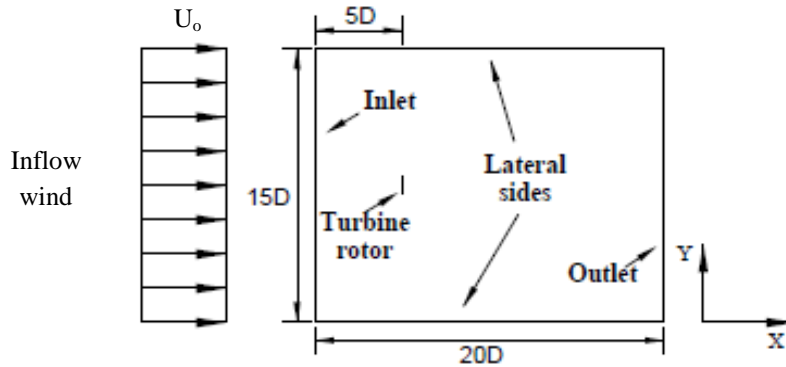


**Fig.1:** Computational domain for single wake case

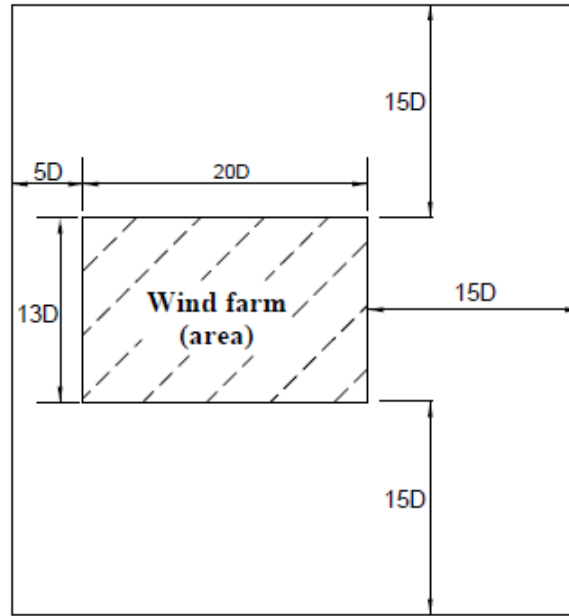


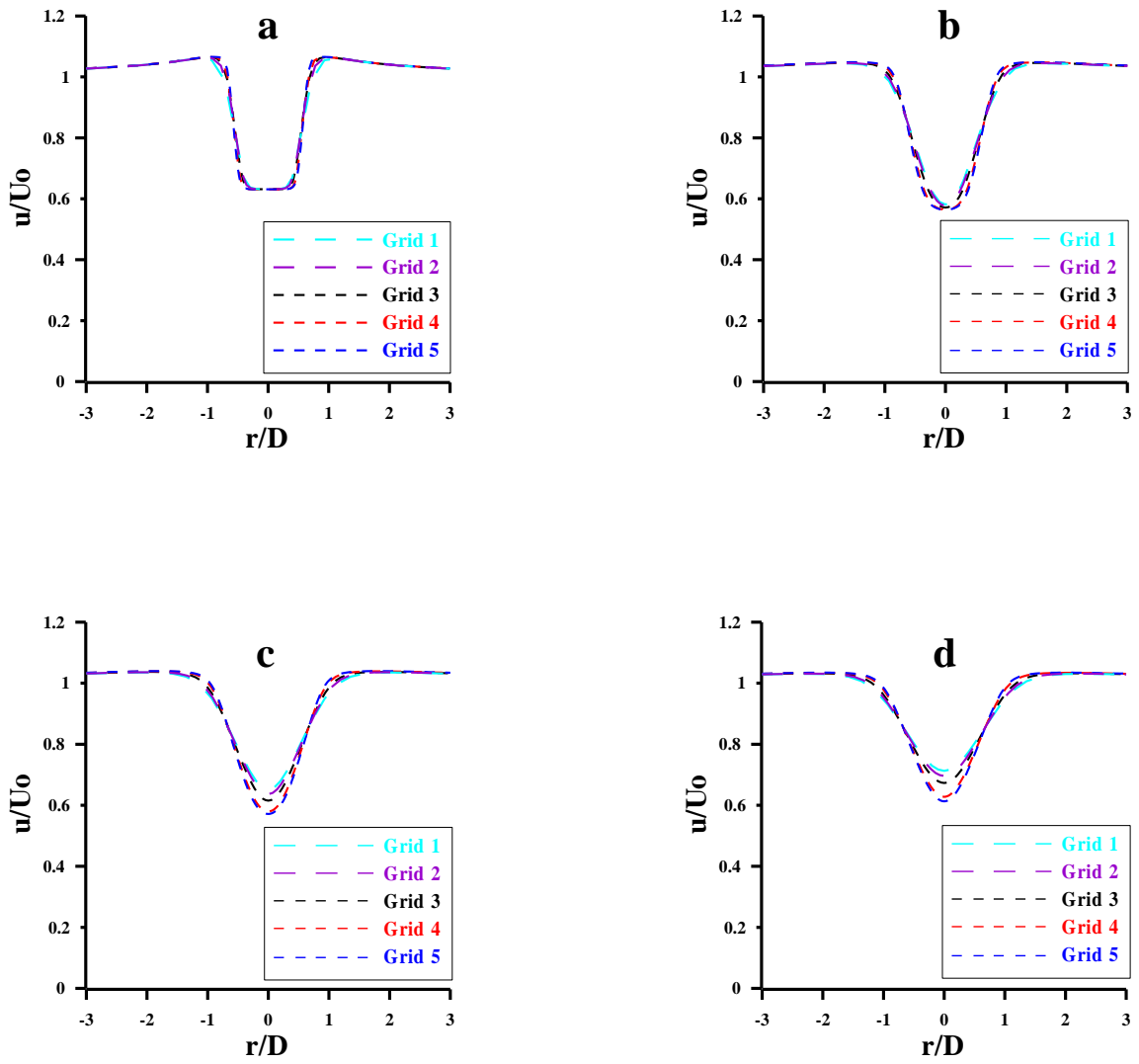
**Fig.2:** Computational domain for wind farm cases with different wind direction

## V. Results and discussion

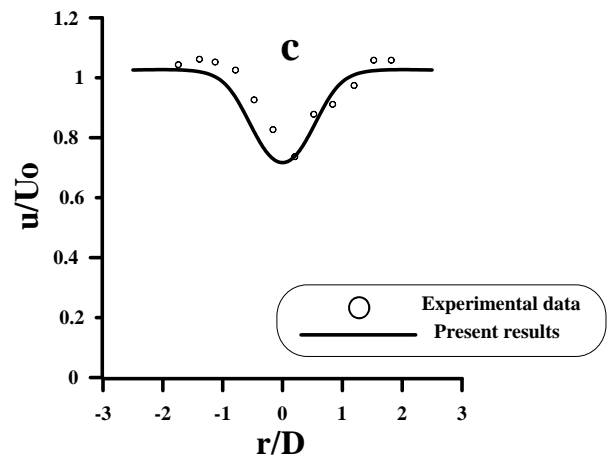
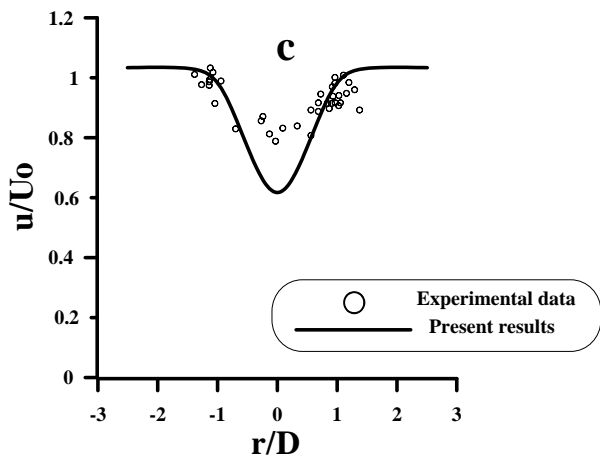
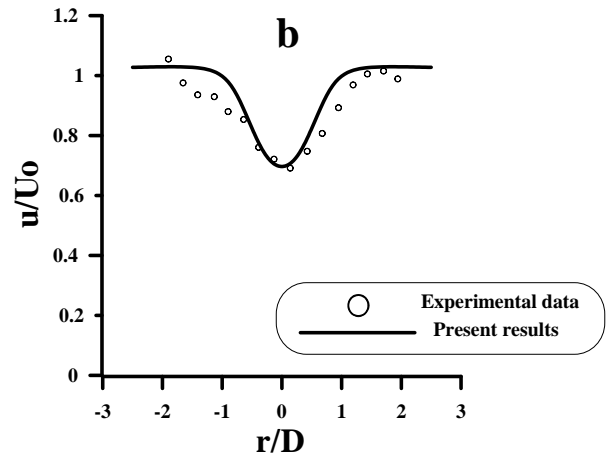
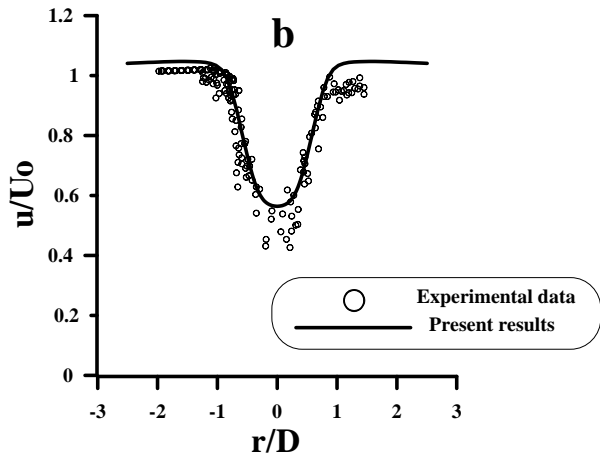
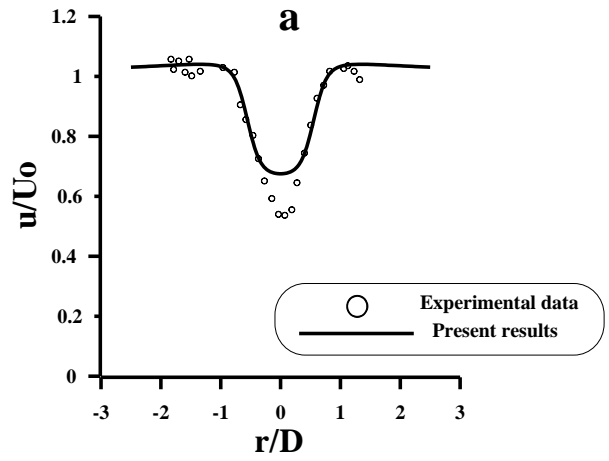
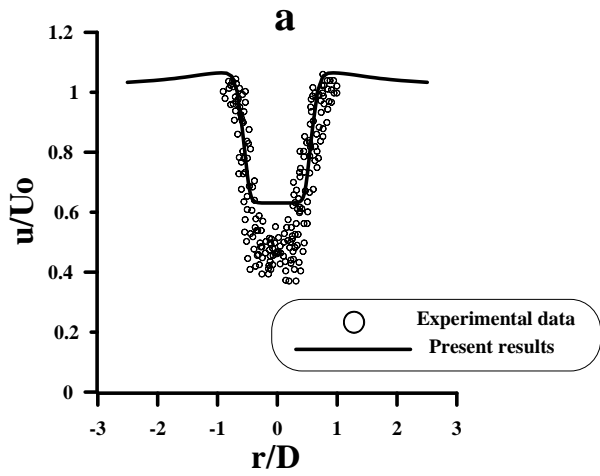
The present numerical methodology is validated through comparison with the experimental data of Danwin turbine [12-13] and Nibe-B turbine [14-15]. The first turbine, Danwin turbine, has rotor diameter of 23 m with hub height of 31 m. The rated power is 180 kW. The data were measured at inflow wind speed of 8 m/s and turbulence intensity of 7% with reported thrust coefficient of 0.82. The second wind turbine, Nibe-B turbine has rotor diameter of 40 m with hub height of 45 m. The data are compared for this turbine at 11.52 m/s inflow wind speed and 10.5% turbulence intensity with 0.67 thrust coefficient. To find the suitable mesh size, five grid resolutions are tested. Grid 1 has 33.1 thousand cells, Grid 2 has 77.9 thousand cells, Grid 3 has 194 thousand cells, Grid 4 has 225 thousand cells and Grid 5 has 896 thousand cells.

Figure 3 presents axial velocity distribution along the wake at different downstream distances. It is shown that the number of grid has no significant effect on results of mean axial velocity up to 4D downstream. However its effect appears at far wake region, at  $x/D=7$  and  $x/D=10$ . Little changes take place due to the use of grid 4 and 5 accordingly grid 4 was used in simulating all the cases. In particular, the turbine rotor is discretized with cell maximum size 0.5 m and the rest of computational domain is discretized with cell of maximum size equals 2 m.

Figure 4 presents the comparison of the present numerical results of axial velocity and the experimental data of Danwin's wind turbine at different distances downstream the turbine. It is seen that the velocity deficit is high in the near wake. An underestimation of predicted velocity is found between the numerical results and measurements in Fig. 4(a). In the far wake the velocity deficit decreases due to turbulent diffusion as shown in Fig. 4(b and c). The predicted velocity is in a good agreement with the experimental data. Furthermore, a comparison of the simulation results and experimental data of Nibe-B turbine is performed as shown in Fig. 5. It is observed that the numerical methodology is acceptable in predicting the wake velocity at far wake region. Hence, it is concluded from the comparisons implemented that El Kasmi model is sufficient to predict the wake behavior, especially in the region of interest,  $x/D$  beyond 4.



**Fig.3:** Danwin turbine: axial velocity distribution for  $U_o = 8$  m/s,  $TI = 7\%$  at: a)  $x/D = 1$ ; b)  $x/D = 4$ ; c)  $x/D = 7$ ; d)  $x/D = 10$



**Fig.4:** Danwin turbine: Flow velocity distribution for  $U_o = 8$  m/s,  $TI = 7\%$  at: a)  $x/D=1$ ; b)  $x/D = 4.15$ ; c)  $x/D = 9.4$  [12-13]

**Fig.5:** Nibe-B turbine: Flow velocity distribution for  $U_o = 11.52$  m/s,  $TI = 10.5\%$  at: a)  $x/D= 2.5$ ; b)  $x/D=6$ ; c)  $x/D= 7.5$  [14-15]

In wind farm simulations, the wind turbines used have the same specifications of the Danwin turbine. The simulations are performed at inflow wind speed of 8 m/s with turbulence intensity of 7%. At this wind speed, the thrust coefficient is 0.82. Three different separation distances, namely 6D, 8D and 10D are used, as shown in Figs. 6, 7, and 8. The lateral side distance is kept constant at 6D. Beside these 3 configurations a fourth configuration of staggered layout of 6D separation distance is also studied as shown in Fig. 9. The dominant wind direction for all configurations is x-direction ( $\Theta_1$ ). Furthermore, the air blowing from three different directions represented by  $\Theta_1$ ,  $\Theta_2$  and  $\Theta_3$  in Figs 6 to 9, is simulated.

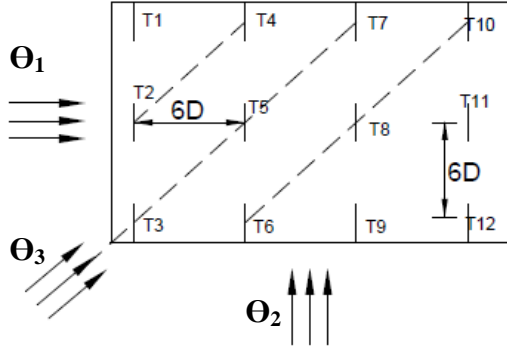


**Fig.6:** Wind farm of non-staggered configuration with 6D separation distance cases ( $C_{11}$ ,  $C_{12}$  and  $C_{13}$ )

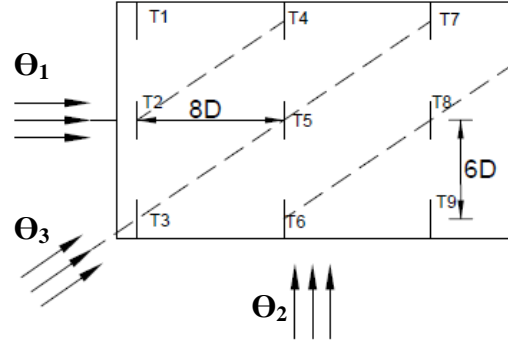


**Fig.7:** Wind farm of non-staggered configuration with 8D separation distance cases ( $C_{21}$ ,  $C_{22}$  and  $C_{23}$ )

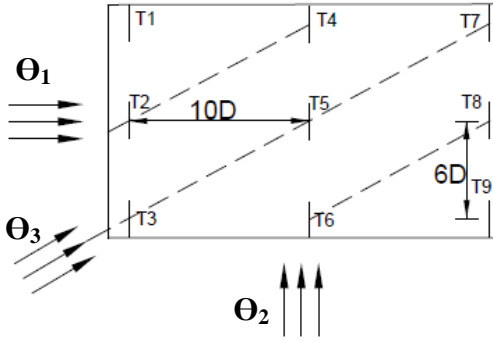


**Fig.8:** Wind farm of non-staggered configuration with 10D separation distance cases ( $C_{31}$ ,  $C_{32}$  and  $C_{33}$ )

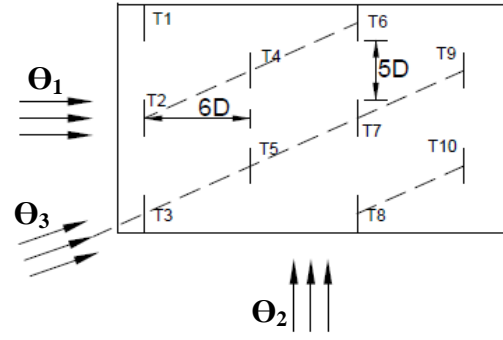


**Fig.9:** Wind farm of staggered configuration with 6D separation distance cases ( $C_{41}$ ,  $C_{42}$  and  $C_{43}$ )

All configurations are represented as  $C_{ij}$ , in which  $i$  is based on the configuration and  $j$  is based on the wind direction as listed in table. 1. It is worth mentioning that there is no yaw misalignment for the different wind directions.

**Table 1:** Abbreviations for all simulated cases of the wind farm

Wind Direction \ Configuration	$\Theta_1=0^\circ$	$\Theta_2=90^\circ$	$\Theta_3=45^\circ$
Non-staggered 6D(1)	$C_{11}$	$C_{12}$	$C_{13}$
Non-staggered 8D (2)	$C_{21}$	$C_{22}$	$C_{23}$
Non-staggered 10D (3)	$C_{31}$	$C_{32}$	$C_{33}$
Staggered 6D (4)	$C_{41}$	$C_{42}$	$C_{43}$

The contours of the axial velocity are presented in Fig. 10, for all configurations, at wind direction  $\Theta_1$ . It is shown that the velocity deficit increases as the flow proceeds downstream the later rows of the wind turbines, up to the third row, as shown in Fig (10-a). However, the fourth row of the wind turbines presents higher velocity recovery as compared to the third row. The cause might be attributed to the increase in the turbulence intensity for the downstream rows. As mentioned in [7]. High turbulence intensity enables a speedy recovery of the velocity in the wake. Furthermore, the wake recovery significantly increases by increasing the separation distance between wind turbines as shown in Fig. 10(a, b and c). That leads to higher inlet velocity to downstream wind turbines.

The staggered distribution shown in Fig (10-d) has a fewer number of wind turbines (10 turbines) in the wind farm compared to the non-staggered distribution, which has 12 turbines. However, the staggered distribution provides more upstream wind turbines. In spite of, the  $6D$  separation distance between first and second row, the second row wind turbines are not affected by the wakes of the first row wind turbines, because the turbines of the first and the second row are not aligned.

The wake behavior is mirrored over any internal wind turbines column. However, the outer column shows different behavior, in which, the mutual effect of the inner column no longer exists. It can be seen from the previously presented Figs. (6-9) that, for the same configuration, the number of WTs columns is different for the different wind directions. For example, in configuration (1) of Fig. 6, the number of columns is 3 for  $\Theta_1$  while it is 6 for  $\Theta_3$ . Hence, Figs (12-15) introduce the axial velocity at the center line of the different columns of wind turbines (referred by CL) for each configuration at the 3 selected wind directions.

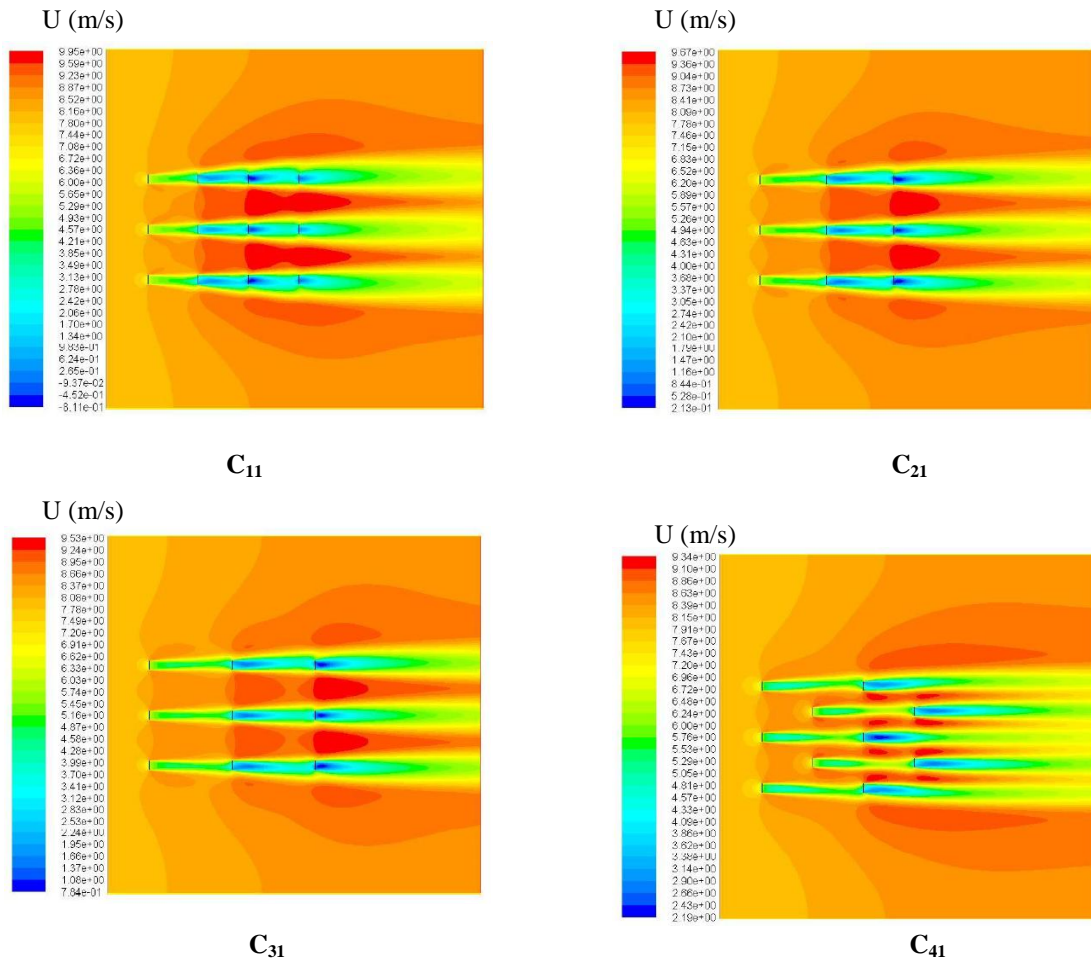


**Fig.10:** Axial velocity contour for all configurations, at wind direction  $\Theta_1$

It is observed that, for non-staggered configuration, the axial velocity at center line is the same for all columns at  $\Theta_1$  and  $\Theta_2$ , see a, b of Figs. 12 to 14. This is because the flow is similar as presented in Fig. 10. However, at wind direction  $\Theta_3$ , the 3 configurations give irregular wind distribution at the center line, as it is much closer to the staggered distribution. Hence, the staggered configuration shows irregular distribution at the different columns as previously shown in Fig. 11.

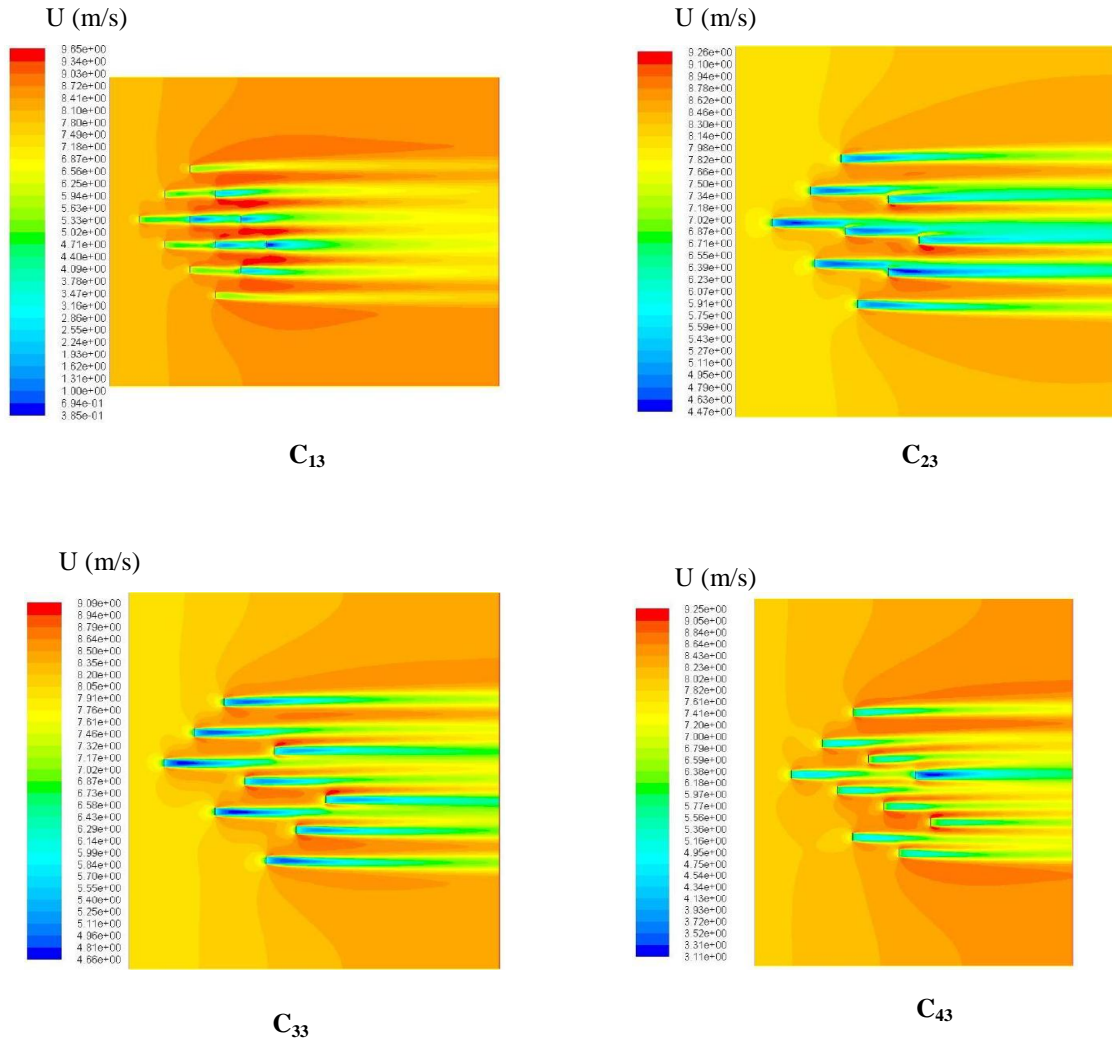
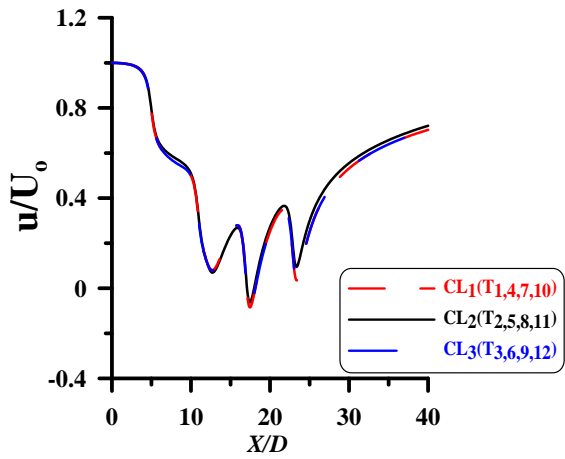
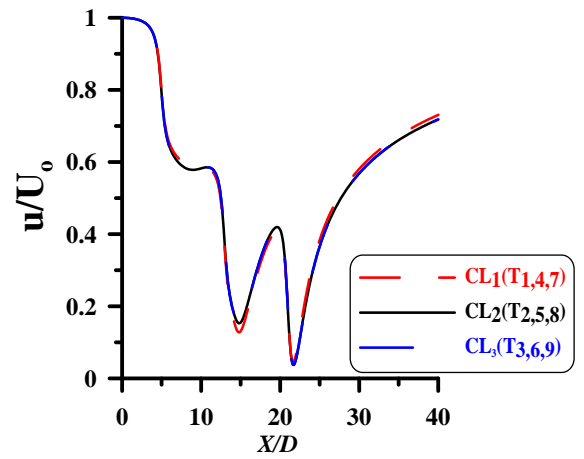


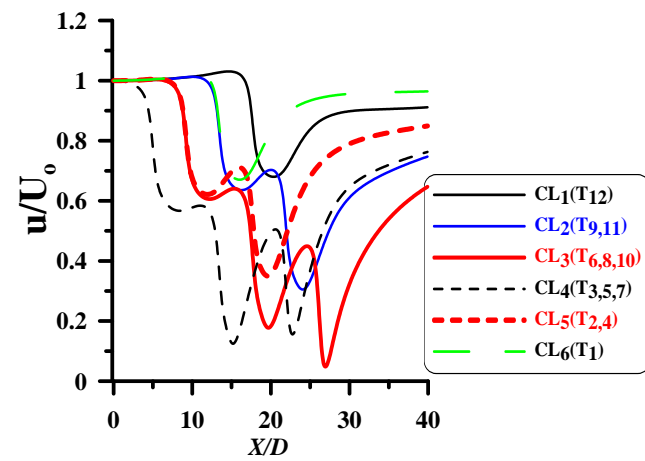
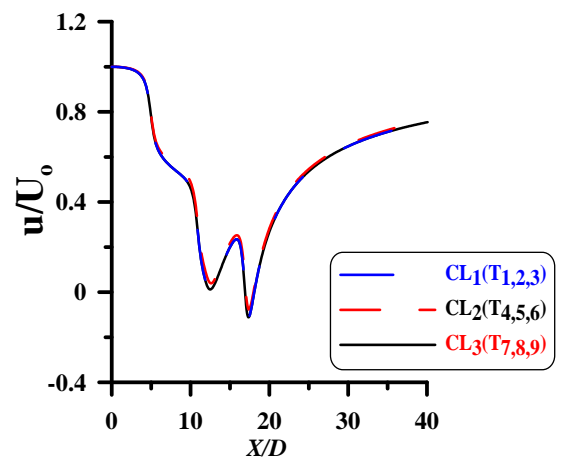
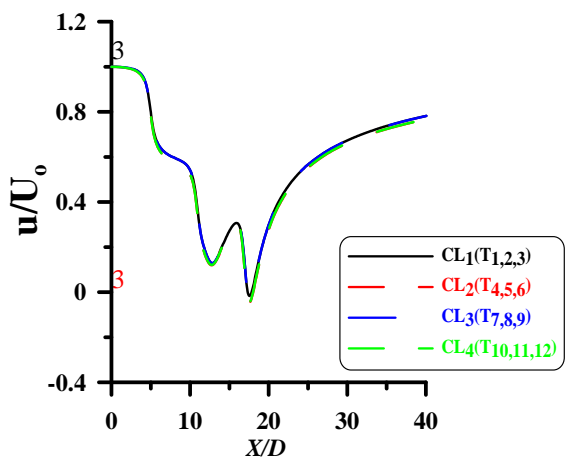
**Fig.11:** Axial velocity contour for all configurations, at wind direction  $\Theta_3$



a)  $\Theta_1$



b)  $\Theta_2$



c)  $\Theta_3$

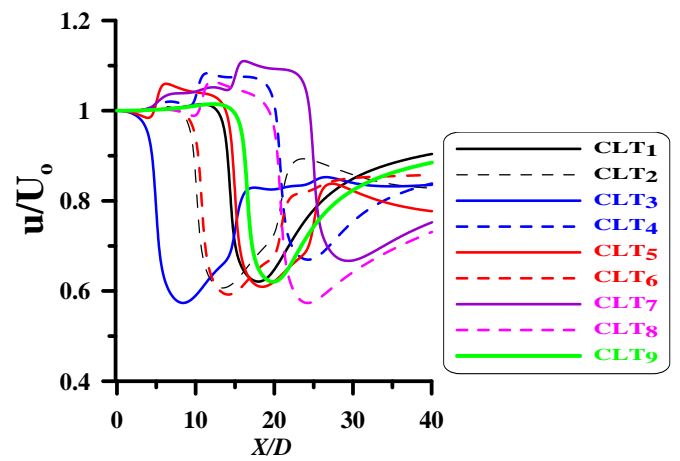
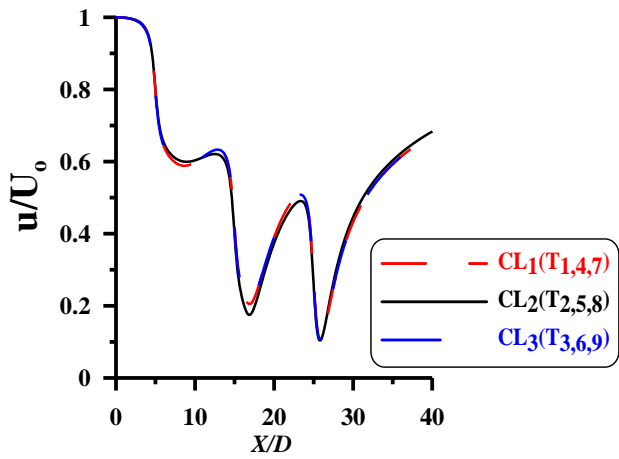
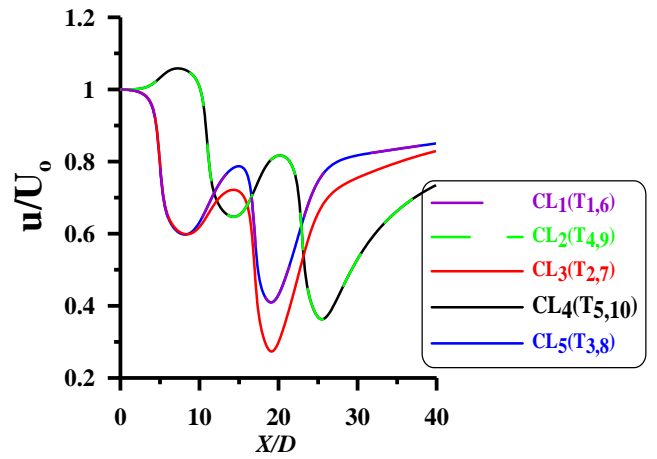


**Fig.12:** Axial velocity distribution along centre lines of wind turbines columns of configuration (1), with 3 different blowing wind directions

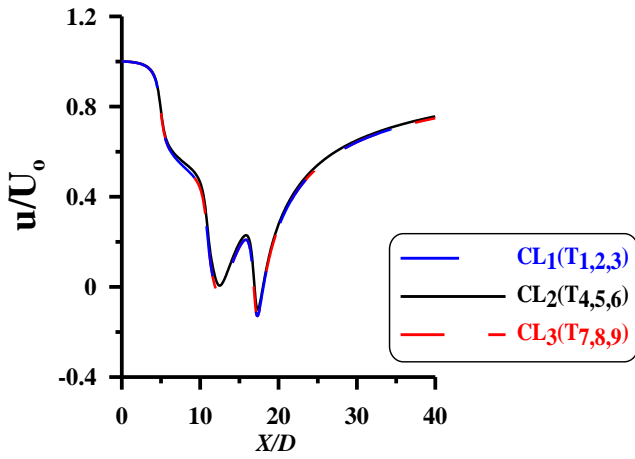
**Fig.13:** Axial velocity distribution along centre lines of wind turbines columns of configuration (2), with 3 different blowing wind directions



a)  $\Theta_1$



b)  $\Theta_2$



c)  $\Theta_3$

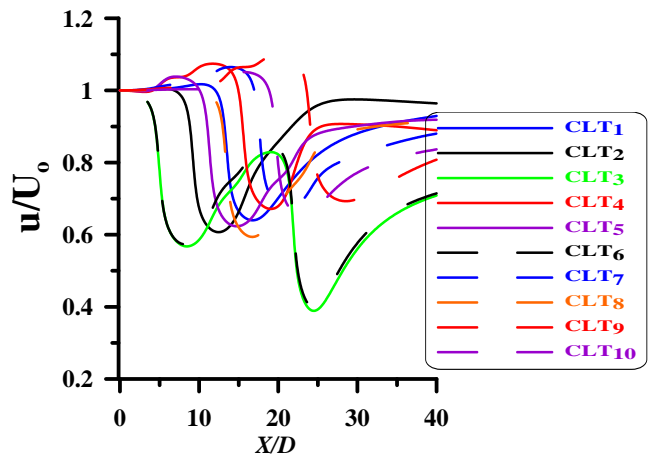
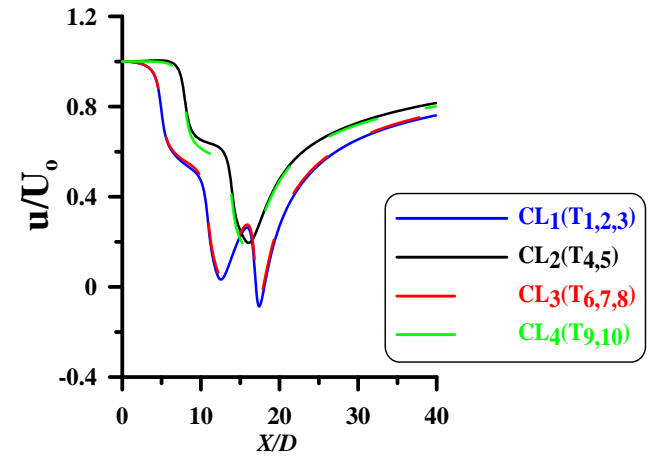


**Fig.14:** Axial velocity distribution along centre lines of wind turbines columns of configuration (3), with 3 different blowing wind directions

**Fig.15:** Axial velocity distribution along centre lines of wind turbines columns of configuration (4), with 3 different blowing wind directions

On the other hand, Table. 2 introduce the wind power available in the wind farm for all the studied cases. The wind power available at each wind turbine is obtained based on the simulation results. Summation of the wind power of all turbines provides the power available in the wind farm. The configurations of non-staggered wind turbines distribution (C2 and C3) give approximated results at all wind directions, configurations 2 and 3. Despite having more WTs, configuration (1) has lower wind power, except at  $\Theta_2$ . It is obvious that the staggered configuration (4) gives the best wind power available for all wind directions, especially in the dominant direction  $\Theta_1$ , see Fig. 16. Furthermore, the power available in the direction  $\Theta_3$  for all configurations is higher than the other two directions. Certainly that happens because the uniform configurations (1, 2 and 3) become closer to the staggered distribution, which leads to more wind turbines without wake effect. Hence, the staggered distribution has the minimum effect of the wakes in reducing the wind power available for the downstream turbines.

## VI. Conclusion

The present CFD results compared well with experimental values especially at far wake. Near wake discrepancies are mainly due to the use of actuator disc model without any wake rotation effects considered.

For wind farm of an area  $13D$  by  $20D$ , CFD simulations are performed using El Kasmi turbulence model. Four configurations have been simulated at three different wind directions. Three non-staggered configurations and one staggered configuration are selected. The results showed that increasing the separation distance leads to a slight increase in the power available in the wind farm, because of the recovery of the wake, which provides higher speeds to the downstream wind turbines. Moreover, the staggered distribution of the wind turbines enhances the power, with less number of turbines. A significant increase in the total power of the wind farm is achieved through the proposed staggered distribution, reaching twice the power of other configurations, at the same wind direction. The wind farm design is not only affected by the separation distance between wind turbines, but also by the distribution method of the wind turbines which are considered a crucial factor in designing the wind farm.

**Table 2:** Power available in the wind for all the wind farm cases of different air directions

Configuration	Number of turbines	Power available at $\Theta_1$ (kW)	Power available at $\Theta_2$ (kW)	Power available at $\Theta_3$ (kW)
(1)Non-staggered 6D	12	477	645	1002
(2)Non-staggered 8D	9	490	444	1180
(3)Non-staggered 10D	9	539	434	1200
(4) Staggered 6D	10	990	628	1315

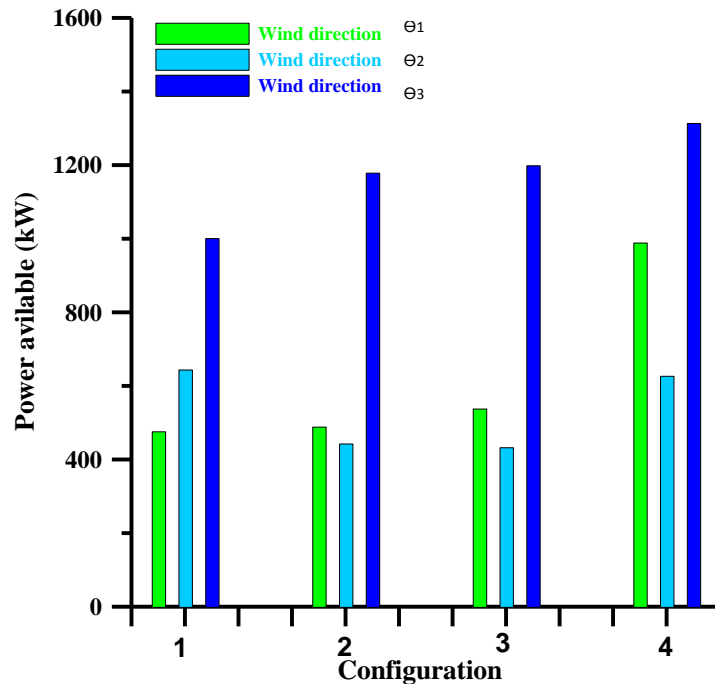


**Fig.16:** Power available in the wind for all the wind farm cases of different air directions

### References

- [1] Gonzalez, J.S., Rodriguez, A.G., Mora, J.C., Santos, J.R., and Payan, M.B., “Optimization of wind farm turbines layout using an evolutive algorithm”, *Renewable Energy*, Vol. 35, no. 8, PP. 1671–1681, 2010.
- [2] Schümann, H., Pierella, F., and Saetran, L., ” Experimental investigation of wind turbine wakes in the wind Tunnel”, *Energy Procedia*, Vol. 35, PP. 285 – 296, 2013.
- [3] Choi, N.J., Nam, S.H., Jeong, J. H., Kim, K.C., “Numerical study on the horizontal axis turbines arrangement in a wind farm: effect of separation distance on the turbine aerodynamic power output”, *J. Wind Eng. Ind. Aerodyn.*, Vol. 117, PP. 11–17, 2013.
- [4] Jourieh, M., Massouh, F., Kuszla, P., Dobrev, I., Maalouf, B.,” Impact of wind turbines interactions on power production”, *19 ème Congrès Français de Mécanique*, PP.24-28, 2009.
- [5] El-Askary, W. A., Sakr, I. M., AbdelSalam, A. M., and Abuhegazy, M. R., “Modeling of wind turbine wakes under thermally-stratified atmospheric boundary layer”, *J. Wind Eng. Ind. Aerodyn.*, Vol. 160, PP. 1–15, 2017.
- [6] Abdelsalam, A. M., Boopathi, K., Gomathinayagam, S., Kumar, S.S., and Ramalingam, V., “Experimental and numerical studies on the wake behavior of a horizontal axis wind turbine”, *J. Wind Eng. Ind. Aerodyn.*, Vol. 128, PP. 54–65, 2014.
- [7] Abdelsalam, A.M., and Ramalingam, V.,” Wake prediction of horizontal-axis wind turbine using full-rotor modeling”, *J. Wind Eng. Ind. Aerodyn.*, Vol. 124, PP. 7–19, 2014.
- [8] Ivanell, S., “Numerical computations of wind turbine wakes”, PhD thesis, KTH Engineering Sciences, 2009.
- [9] Enrico, C.,CFD-RANS Study of Horizontal Axis Wind Turbines, PhD Thesis University of Cagliari, Department of Mechanical Engineering, 2009.
- [10] El Kasmi, A., and Masson, C., “An extended k–ε model for turbulent flow through horizontal-axis wind turbines,” *J. Wind Eng. Ind. Aerodyn.*, Vol. 96, PP.103–122. 2008.

- [11] Crespo, A., Manuel, F., Moreno, D., Fraga, E., and Hernandez, J., "Numerical analysis of wind turbine wakes", In: Proceedings of Delphi Workshop on Wind Energy Applications, Delphi, Greece, pp. 15–25, 1985.
- [12] Magnusson, M., and Smedman, A. S., "Air flow behind wind turbines", *J. Wind Eng. Ind. Aerodyn*, Vol. 80, PP. 169–189, 1999.
- [13] Magnusson, M., Rados, K.G., and Voutsinas, S.G., "A study of the flow downstream of wind turbine using measurements and simulations", *Wind Eng.*, Vol. 20, PP. 389-403, 1996.
- [14] Pederson, B.M., and Nielson, P., "Description of the two Danish 630 kW wind turbines, Nibe-A and Nibe-B, and some preliminary test results", DEFU, Denmark. In: Third International Symposium on Wind Energy Systems, pp. 223–238, 1980.
- [15] Taylor, G.J., Milborrow, D.J., McIntosh, D.N., and Swift-Hook, D.T., "Wake measurements on the Nibe windmills", In: Proceedings of Seventh BWEA Wind Energy Conference, Oxford, pp. 67–73, 1985.